Unraveling Specific Brain Microstructural Damage in Moyamoya Disease Using Diffusion Magnetic Resonance Imaging and Positron Emission Tomography

Shoko Hara, MD,*,† Masaaki Hori, MD, PhD,† Ryo Ueda, MS,† Shihori Hayashi, MD, PhD,*,‡ Motoki Inaji, MD, PhD,*,‡ Yoji Tanaka, MD, PhD,* Taketoshi Maehara, MD, PhD,* Kenji Ishii, MD,‡ Shigeki Aoki, MD, PhD,† and Tadashi Nariai, MD, PhD*,‡

Background and Purpose: Chronic ischemia may induce brain microstructural damage and lead to neurocognitive dysfunction in patients with Moyamoya disease (MMD). We applied neurite orientation dispersion and density imaging (NODDI) and ^{15}O-gas positron emission tomography (PET) to elucidate the specific ischemic brain microstructural damage of MMD in the cortex and the white matter. *Materials and Methods:* Thirty-one patients (16-63 years old, 9 males) and 20 age- and sex-matched normal controls were enrolled in this study. NODDI evaluates quantitative parameters reflecting neurite and axonal density, network complexity and the interstitial fluid in all participants. Of 31 patients, 12 newly diagnosed patients were evaluated with PET, also. We evaluated correlations between the microstructural parameters of NODDI and the hemodynamic and metabolic parameters of PET, the relationship between NODDI and clinical severity of each hemisphere (Normal, Asymtpomatic, Symptomatic, and Infarcted) as well as neurocognitive performance. *Results:* All NODDI parameters significantly correlated with PET parameters (absolute $r = 0.46$-0.83, $P \leq .048$) and clinical severity ($P < .001$), suggesting that neurite and axonal density and network complexity decreased, and the interstitial fluid increased, as the ischemic burden became severe. NODDI parameters reflecting neurite and axonal density and network complexity significantly correlated with neurocognitive profiles ($r = 0.36$-0.64, $P \leq .048$), but the interstitial fluid component did not. *Conclusions:* Chronic ischemia in patients with MMD may induce decreased neurite and axonal density, simplified network complexity, and may lead to neurocognitive dysfunction. The increased interstitial fluid accompanying hemodynamic impairment may not be identical to the decreased neurite density and might be driven by another mechanism.

Key Words: Moyamoya disease—ischemia—cerebral blood flow and metabolism—diffusion MRI—magnetic resonance imaging—cognition—cognitive impairment

From the *Department of Neurosurgery, Tokyo Medical and Dental University, Bunkyo-ku, Tokyo, Japan; †Department of Radiology, Juntendo University, Bunkyo-ku, Tokyo, Japan; and ‡Team for Neuroimaging Research, Tokyo Metropolitan Institute of Gerontology, Itabashi-ku, Tokyo, Japan.

Received September 9, 2018; revision received December 4, 2018; accepted December 27, 2018.

Financial support: This work is supported by Grants-in-Aid for Scientific Research "KAKENHI", the Japan Society for the Promotion of Science (Grant #16K19995 and #16H06280).

Address correspondence to Shoko Hara, Department of Neurosurgery, Tokyo Medical and Dental University, 1-5-45 Yushima, Bunkyo-ku, Tokyo 113-8519, Japan. E-mail: shara.nsrg@tmd.ac.jp.

1052-3057/$ - see front matter

https://doi.org/10.1016/j.jstrokecerebrovasdis.2018.12.038

Introduction

Moyamoya disease is characterized by a progressive occlusion of the intracranial arteries in the circle of Willis,[1] primarily affecting children and young adults. Cognitive dysfunction occurs in these patients, even without stroke episodes[2] and conventional magnetic resonance imaging (MRI) sequences are not sufficient to evaluate the ischemic disease burden of these patients.[3,4] Therefore, it is necessary to establish some advanced imaging technique to evaluate the ischemic burden of these patients so as to decide the most appropriate surgical and nonsurgical treatment.

Advanced MRI techniques such as diffusion-weighted imaging such as diffusion tensor imaging (DTI)[4] have been applied to detect brain microstructural ischemic damage in Moyamoya disease that cannot be detected by conventional morphological MRI. These studies suggested that chronic ischemia induced by Moyamoya disease leads to white matter microstructural damage, and thus leads to neurocognitive dysfunction. However, parameters of previously reported diffusion metrics (eg, the fractional anisotropy [FA] of DKI) did not directly reflect specific microstructural features in individual tissues.

Recently, a multishell diffusion MRI technique called neurite orientation dispersion and density imaging (NODDI), which can be acquired in a clinically feasible scan time, has been proposed to evaluate brain microstructure in both the cortex and the white matter.[5] In the NODDI model, 3 microstructural environments are distinguished (intracellular, extracellular, and cerebrospinal fluid [CSF] compartments), and the Watson distribution is adopted to model highly dispersed neuritic structures, such as dendritic trees in the gray matter. NODDI obtained 3 parameters: intracellular volume fraction (V_{ic}) represents the density of axons and dendrites based on intracellular diffusion; the orientation dispersion index (OD) represents the dispersion of axons and dendrites in the intracellular component; and isotropic volume fraction (V_{iso}) reflects the interstitial fluid component in the brain parenchyma. Thus far, numerous studies using NODDI have revealed correlations among the histological microstructure[6,7] and have evaluated stroke,[8] neurodegenerative diseases,[9,10] and psychotic disorders.[11] A recent study using NODDI suggested microstructural damage in patients with Moyamoya disease compared to normal controls and its correlation with neurocognitive dysfunction.[3] However, the correlation between MRI parameters and the quantitative hemodynamic and metabolic parameters obtained using ^{15}O-gas positron emission tomography (PET) has yet to be evaluated in this disease population.

The aim of this study is to elucidate specific ischemic brain microstructural damage and the mechanism of neurocognitive dysfunction in patients with Moyamoya disease by analyzing the relationship among specific microstructural parameters of NODDI and ^{15}O-gas PET parameters (cerebral blood flow [CBF], cerebral blood volume [CBV], mean transit time [MTT], oxygen extraction fraction [OEF], and cerebral metabolic ratio of oxygen [CMRO2]), clinically assessed disease severity of the hemispheres, and neurocognitive dysfunction. Specifically, we hypothesized that as the ischemic burden became severe, V_{ic} would decrease and OD and V_{iso} would increase, as reflections of the decreased neurite and axonal density, disorganized and randomized network structure, and increased interstitial fluid. In concordance with the hemodynamic compromise theory,[12] we expected that as CBF and CMRO2 decreased and CBV, MTT, and OEF increased, V_{ic} would decrease and OD and V_{iso} would increase.

Materials and Methods

Study Design

The ethical committees of Tokyo Medical and Dental University (M2000-2302) and Juntendo University (16-100) approved this prospective study protocol, which was registered with the University Hospital Medical Information Network Clinical Trials Registry (UMIN-CTR ID: 000023082). Patients diagnosed with Moyamoya disease according to the diagnostic guideline[1] were recruited in this study and evaluated using an MRI protocol, including NODDI, and the neuropsychological test, Wechsler Adult Intelligence Scale-III (WAIS-III). All participants were free of focal sensory and motor disturbances, although 4 participants had partial or complete hemianopia from occipital infarction, and independent activities of daily living with a modified Rankin Scale score of 0-3. Due to the invasive nature of PET, we performed a PET scan only in patients who required further detailed examination of cerebral hemodynamics to confirm a possible surgical indication. In addition to the Moyamoya patients, healthy normal volunteers without a history of neurological and severe systemic disease who were age- and sex-matched to the patients were recruited and evaluated using the same MRI protocol. Written informed consent was obtained from all participants after a detailed explanation of the study protocol was provided. An experienced neuroradiologist (M.H.) who was blinded to the clinical history of the participants assessed the presence of infarctions, hemorrhage, and white matter T2 hyperintensities and the absence of acute ischemic lesions by a visual inspection of conventional MRI images, ie, diffusion-weighted imaging, fluid attenuated inversion recovery imaging, susceptibility-weighted imaging and magnetic resonance angiography.

Patients With Moyamoya disease

Between September 2015 and May 2017, 31 patients over 16 years of age (16-63 years; average 40 years, 9

males and 1 left-handed) were enrolled in this study. The participants included 8 patients with cortical infarctions and 11 patients with white matter infarctions that were visible on conventional MRI images; 1 patient with a history of intraventricular hemorrhage; and 9 patients who underwent an indirect bypass surgery in our university hospital more than 1 year before the MRI exam. According to the clinical histories of the patients, 11 patients had childhood-onset (onset at ≤15 years of age) and 20 patients had adult-onset (onset at ≥16 years of age) disease.

Of all the patients, 12 newly diagnosed patients who had not undergone an operation were evaluated by PET. These patients comprised 4 males aged 21-61 years (42 years on average). The interval between the PET and MRI exams was 28 days on average (0-73 days) while their symptoms were unchanged, and no new lesions appeared in the subsequent imaging exam. Complete patient details are shown in Supplementary Table 1.

According to the clinical information, both hemispheres of all participants were categorized into the following 4 groups by the consensus of 2 authors (S.H. and T.N.): Normal (N), Asymptomatic (A), Symptomatic (S), and Infarcted (I). Group N included both hemispheres of the healthy volunteers and the healthy hemispheres (ie, no vascular lesions) of patients with unilateral disease. All hemispheres harboring cortical or large (>10 mm) white matter infarctions were categorized into group I. Group S included hemispheres with focal ischemic symptoms and/or hemodynamic impairment, as confirmed by either PET or perfusion MRI (see Supplemental Method for details). The remaining hemispheres with mild hemodynamic changes and postoperative sides were categorized into group A.

Neuropsychological Assessment

Clinical neuropsychologists from our university hospital administered the WAIS-III to each patient using a standardized Japanese version published in 2007 (Nihon Bunka Kagakusha Co., Ltd. Tokyo, Japan). The full-scale intelligence quotient (FIQ), verbal quotient IQ (VIQ), performance IQ (PIQ), and 4 index scores, ie, verbal comprehension index (VC), working memory index (WM), perceptual organization index (PO), and processing speed index (PS) adjusted for age were recorded.

Healthy Volunteers

Twenty normal healthy volunteers who were age- and sex-matched to the patients were recruited in this study and evaluated concordantly with the patients. They were aged 17-61 years old (39 years on average) and included 6 males and 1 left-handed individual. Four of the 20 subjects exhibited small T2 hyperintensities (<3 mm) in the white matter, which were assessed as nonspecific or age-related changes by an experienced neuroradiologist (M.H.).

MRI Acquisition and Computation of Parametric Maps

All MRI data were acquired using a 3T system with a 32-multichannel receiver head coil (MAGNETOM Skyra, Siemens, Germany). All participants were evaluated using fluid attenuated inversion recovery (TR = 12000 ms, TE = 96 ms, flip angle = 150°, TI = 2750 ms, slice thickness = 3 mm, gap = 0.6 mm), and susceptibility-weighted imaging (TR = 27 ms, TE = 20 ms, flip angle = 15°, slice thickness = 1.6 mm, gap = 0 mm) was acquired to evaluate the presence of infarctions and hemorrhage.

Diffusion-weighted images were acquired using a fat-saturated single-shot echo planar imaging sequence (TR = 4500 ms; TE = 105 ms; flip angle = 90°; voxel size = $2 \times 2 \times 2$ mm^3; acquisition matrix = 100; number of slices = 90, multiband factor = 2; *b*-values and axes: 0, 700: 30 axes, 2850: 60 axes). The data were collected using reversed phase-encoded blips, resulting in pairs of images with distortions oriented in opposite directions. The acquisition time for the diffusion-weighted images was approximately 8 minutes 38 seconds for the main images and 1 minutes 37 seconds for the reversed phase. Using these pairs, the susceptibility-induced off-resonance field was estimated using a method similar to that described elsewhere,[13] as implemented in FMRIB Software Library version 5.0,[14] and the 2 images were combined into a single corrected image. The data were then fit with the NODDI model using the NODDI MATLAB toolbox (https://www.nitrc.org/projects/noddi_toolbox/) to create parametric maps of V_{ic}, OD and V_{iso} according to a theory described elsewhere.[5]

Three-dimensional T1-weighted images (TIWI) prepared via rapid acquisition with a gradient echo sequence (TR = 1700, TE = 2.61, flip angle = 10°, TI = 800, parallel imaging using GeneRalized Autocalibrating Partial Parallel Acquisition;) were acquired and voxelwise calculated for the probability of the gray matter and white matter segment using the standard segment function of SPM12 (http://www.fil.ion.ucl.ac.uk/spm/) in the MATLAB 2016a environment (The MathWorks Inc., Natick, MA).

PET Data Acquisition and Computation of Parametric Maps

PET data were acquired using a Discovery 710 PET/CT scanner (GE Healthcare, Milwaukee, WI). After a low-dose CT scan was performed for attenuation correction, 3 sequential emission scans of inhaled $C^{15}O_2$ (2000 MBq/min), $^{15}O_2$ (3000 MBq/min) and CO^{15} (2000 MBq/min) were conducted using a neck shield. The 3.5-minutes acquisition in the $C^{15}O_2$ and $^{15}O_2$ scans was initiated simultaneously with a 1.5-minutes inhalation of these gases.[15] Then, the participants inhaled $C^{15}O$ gas for 3

minutes and were scanned for 4 minutes. The amounts of radioactivity in the arterial whole blood were manually collected at 0, 2, and 4 minutes, while images of inhaled $C^{15}O_2$ and $^{15}O_2$ were acquired.[16]

The PET images were reconstructed under the following conditions: 3-dimensional-ordered-subset expectation-maximization algorithm, 128 × 128 matrix, 47 slices, 2.0 mm/pixel, 3.27 mm/slice, 4 iterations, 16 subsets, and Gaussian filter of 3.0 mm (FWHM). The clinical $C^{15}O_2$ and $^{15}O_2$ images consisted of 12 frames of 5 seconds and 10 frames of 15 seconds, and the attenuation was corrected using the corresponding computed tomography image. The scatter correction algorithm used a scatter limitation correction.[17] We calculated the CBF, CBV, CMRO2, and OEF according to the functional images and amounts of radioactivity in the arterial blood using the PET autoradiographic method with Xeleris software (GE Healthcare, Milwaukee, WI).[18] The final spatial resolution of the CBF, CBV, CMRO2, and OEF maps was 5.78 mm.

Postprocessing of Parametric Maps

The following steps were performed using MRIcron (http://www.fil.ion.ucl.ac.uk/spm/software/spm12/). Before postprocessing, all NODDI and PET parametric maps were visually inspected to ensure appropriate quality. Since many patients had focal lesions and/or global atrophies that negatively affected the precision of normalization, we registered each map to the native space of the same patient to avoid the effect of deformation that inevitably accompanies normalization. Because the PET data had the lowest spatial resolution, we reorganized all the MRI data to the same spatial resolution as that of PET. MTT maps were created by calculating the CBV/CBF values on a voxel-by-voxel basis.

First, signals outside the brain parenchyma (including CSF signals in the ventricles and the artifacts at the frontotemporal base) in all the NODDI maps were deleted using CSF mask created from the V_{iso} images and the brain parenchyma mask created from the b0 images. Then, all NODDI maps were coregistered to the TIWI of each patient using the same transformation matrix as that of the b0 image. For patients with PET exams, the NODDI maps and the gray/white matter segments created from T1WI were coregistered to the CBF images from PET using the same transformation matrix as that used for the T1WI. For patients and healthy volunteers without PET exams, the NODDI maps and gray and white matter segments were simply resliced to the size of the PET (128 × 128 matrix, 47 slices, 2.0 mm/pixel, 3.27 mm/slice). The accuracy of the registration in each patient was visually confirmed (Supplementary Figure 1). To match the spatial resolution of PET,[19] a 2D Gaussian smoothing operator of FWHM = 5.42 mm and 5.69 mm was applied to the NODDI parametric maps and gray/white matter segments, respectively.

Regions of Interest

We created regions of interest that cover the cortex and the white matter area of each patient using the gray and white matter segments created from the T1WI. First, by segmentation function of SPM12, maps of the probability of each voxel (ranging from 0 to 1) belonging to gray matter and white matter were created. To mitigate the partial volume effect, thresholds of 0.6 for the gray matter and 0.9 for white matter were applied. Since these segments include the cerebellum, the brainstem and the basal ganglia, these regions were manually removed to focus on the cerebral hemispheres. To minimize the partial volume effect of each region (ie, exclusion of CSF and gray matter from the white matter mask and exclusion of CSF and white matter from the cortical mask) and to correct registration errors, the masks were overlaid on the NODDI maps and further modified. For patients with PET exams, the sinus artifact on the CBV images was also avoided so in order to only calculate regional values of brain parenchyma.

Because we aimed to evaluate the quantitative values of the normal-appearing brain parenchyma, the cortical and white matter masks were manually modified to avoid cortical and/or white matter lesions and/or infarctions visible on the conventional MRI and b0 images and the area with very low CMRO2 values suggesting the regions were nonfunctional. Manual correction of masks is necessary because automated segmentation of SPM12 frequently misclassify the infarcted lesion as the cortex or white matter, depending on the signal intensity of T1WI. Finally, the images were divided into the right and left sides. The whole brain and hemispheric values of all NODDI and PET parametric maps were calculated for each patient using the fslstats function in the FMRIB Software Library.

Statistical Analysis

All statistical analyses were performed using JMP ver. 12.0.1 (SAS Institute, Cary, NC). Because of our small sample size, we presumed that the PET and NODDI parameters were normally distributed based on studies involving larger samples.[6,20] In all analyses, P values $< .05$ (with or without Bonferroni correction) were considered significant.

First, we analyzed the regional values of the patients with PET exams and calculated the Pearson's correlation coefficients among the NODDI parameters (V_{ic}, OD, and V_{iso}) and PET parameters (CBF, CMRO2, MTT, CBV, and OEF) in cortical and white matter areas. Regarding the CBV values, a log transformation was applied because CBV has been reported to have a skewed distribution due to the augmentation of the vasculature by Moyamoya vessels.[20] The correlation among the PET parameters of the cortex and the NODDI parameters of the white matter in the same hemisphere was also investigated.

Next, the V_{ic}, OD and V_{iso} values in each hemisphere group (N, A, S, and I) and the age distribution were calculated and compared using the Tukey-Kramer honestly significant difference test (TK-HSD) and Jonckheere-Terpstra trend test (J-T). The percentage of white matter hyperintensities and lesions in group A, S, and I were calculated and compared using the T-K HSD test. The age, sex, and estimated onset of the disease of each group are summarized in Table 1. The correlation among V_{ic}, OD, V_{iso}, and age, and the difference of these parameters according to the estimated onset from the clinical history was also evaluated.

Finally, the correlations between the whole-brain NODDI parameters and WAIS-III profiles were evaluated. The score distributions of the VIQ, PIQ, and the 4 index scores were calculated and compared using the unpaired t test and T-K HSD test, and the number of patients falling $>$ 1 or 2 standard deviations from the mean were counted. To account for possible lateralization effects, the NODDI values of the left and right hemispheres and the correlations among the neuropsychological scores and the NODDI parametric values were evaluated.

Details of the methods, results and supplemental analyses are available in the ONLINE SUPPLEMENTAL MATERIAL, and the full dataset is available from the corresponding author upon reasonable request.

Results

NODDI and PET in Moyamoya Patients

Figure 1 illustrates each parametric map of a representative case.

In the cortical areas (Fig 2), OD values significantly correlated with all PET parameters, particularly with CBF and MTT, except for OEF. A significant correlation was also observed between V_{ic} and MTT, in addition to between V_{iso} and CBF, MTT and CBV. The correlation between OD and CBF/MTT and between V_{iso} and MTT remained significant after Bonferroni correction of the P value. Only OD exhibited significant positive correlation with CMRO2, which was not significant after Bonferroni correction.

In the white matter area (Fig 3), V_{ic} showed a better negative correlation with PET parameters than with OD, as in contrast to the cortical areas. V_{iso} positively correlated with the MTT and CBV, which is similar to the correlation observed in the cortical areas.

Correlation analysis between cortical PET parameters and white matter NODDI parameters revealed significant correlations between V_{ic} and CBF/MTT ($r = -0.45$; $P = .03$ and $r = -0.46$; $P = .02$) and between V_{iso} and CBF, CBV and MTT ($r = -0.48$; $P = .02$, $r = 0.43$; $P = .04$ and $r = 0.60$; $P = .002$, Supplementary Table 5). However, no correlation was observed between any NODDI parameters and CMRO2.

Table 1. *Background information of the 4 groups. There was no significant difference of age, sex, and estimated disease onset among four groups. White matter T2 hyperintensities were more frequent in other 3 groups compared to group Normal (N)*

	Clinical severity	No. of hemispheres (total: 102)	Age		Sex		Estimated onset	White matter T2 hyperintensities	
			Median (range)		No. of male (%)		No. of adult onset (%)	No. of hemispheres (%)	
Normal ($n = 20$)	Normal (N)	40	40 (17-64)	40 (17-64)	13 (30)	12 (30)	-	7 (7)	7 (18)
Moyamoya ($n = 31$)		4		44 (19-61)		1 (25)	1 (25)		0 (0)
	Asymptomatic (A)	25	44 (16-63)		5 (20)		7 (28)	**17*** **(68)**	
	Symptomatic (S)	15	42 (16-61)		4 (27)		5 (33)	**9*** **(53)**	
	Infarcted (I)	18	38 (16-50)		6 (33)		9 (50)	**15*** **(83)**	

*$P < .05$ (unpaired T-test, between Normal and others).

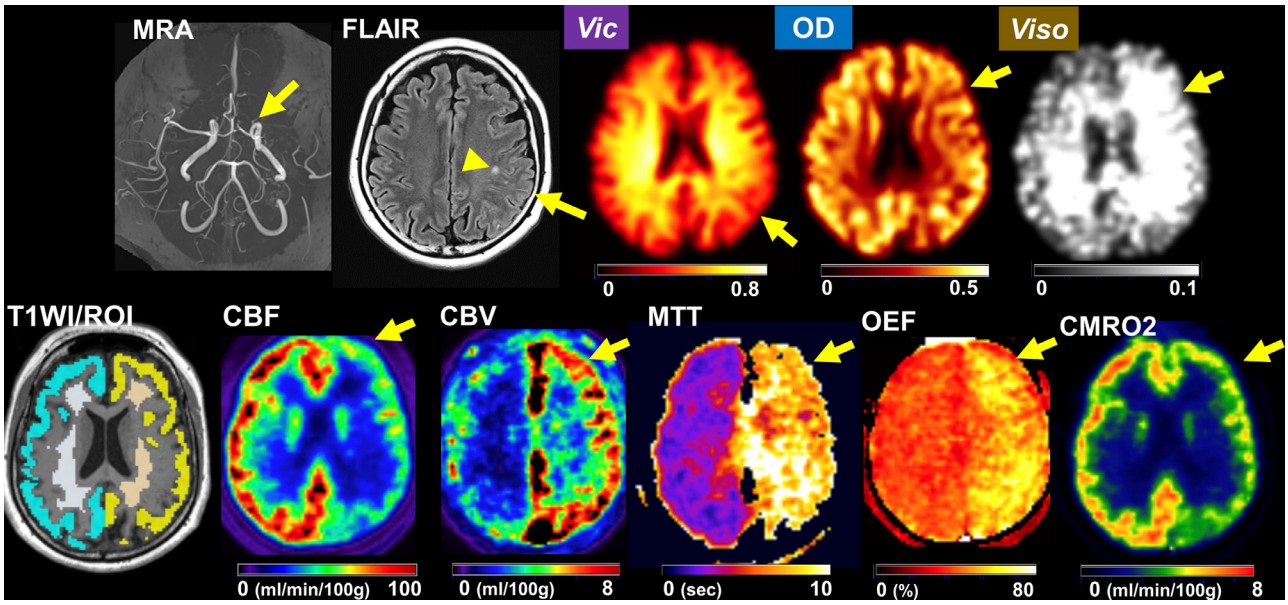

Figure 1. *A 42-year-old female who presented with transient right hemiparesis. Magnetic resonance angiography (MRA) revealed a stenosed terminal portion of the left internal carotid artery, an occluded left middle cerebral artery and left anterior cerebral artery, whereas the artery on the right side was unaffected. The fluid attenuated inversion recovery (FLAIR) image revealed small white matter hyperintensities (arrowhead) and cortical vessel hyperintensity ('ivy sign') in the left parietal lobe (arrow). Visually, the orientation dispersion index (OD) was decreased and isotropic volume fraction (V_{iso}) were increased in the left frontal lobe (arrow), and positron emission tomography (PET) images showed decreased cerebral blood flow (CBF) and cerebral metabolic rate of oxygen (CMRO2), as well as increased cerebral blood volume (CBV), mean transit time (MTT) and oxygen extraction fraction (OEF). The laterality of the intracellular volume fraction (V_{ic}) was visually less apparent but was suggested in the white matter of the parietal lobe (arrow). The regions of interests (ROIs) were created from the segmented T1-weighted images (TIWI; see Materials and Methods for details) to avoid the cortical and white matter lesion that was apparent on the conventional imaging.*

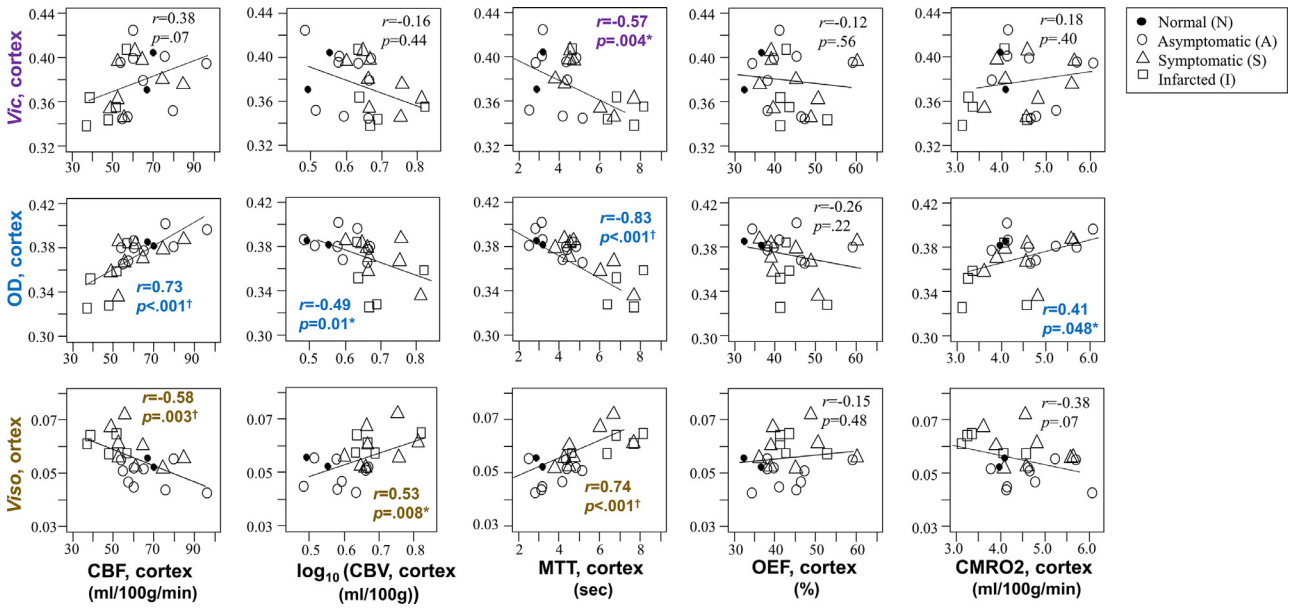

Figure 2. *The correlations among the parametric values of neurite orientation dispersion and density imaging (NODDI) and positron emission tomography (PET) in the cortex.*

*The orientation dispersion index (OD) appeared to correlate best with the hemodynamic and metabolic parameters, particularly cerebral blood flow (CBF) and mean transit time (MTT). *P < .05 and †P < .05 after Bonferroni correction. CBV, cerebral blood volume; CMRO2, cerebral metabolic rate of oxygen; OD, orientation dispersion index; OEF, oxygen extraction fraction; V_{ic}, intracellular volume fraction.*

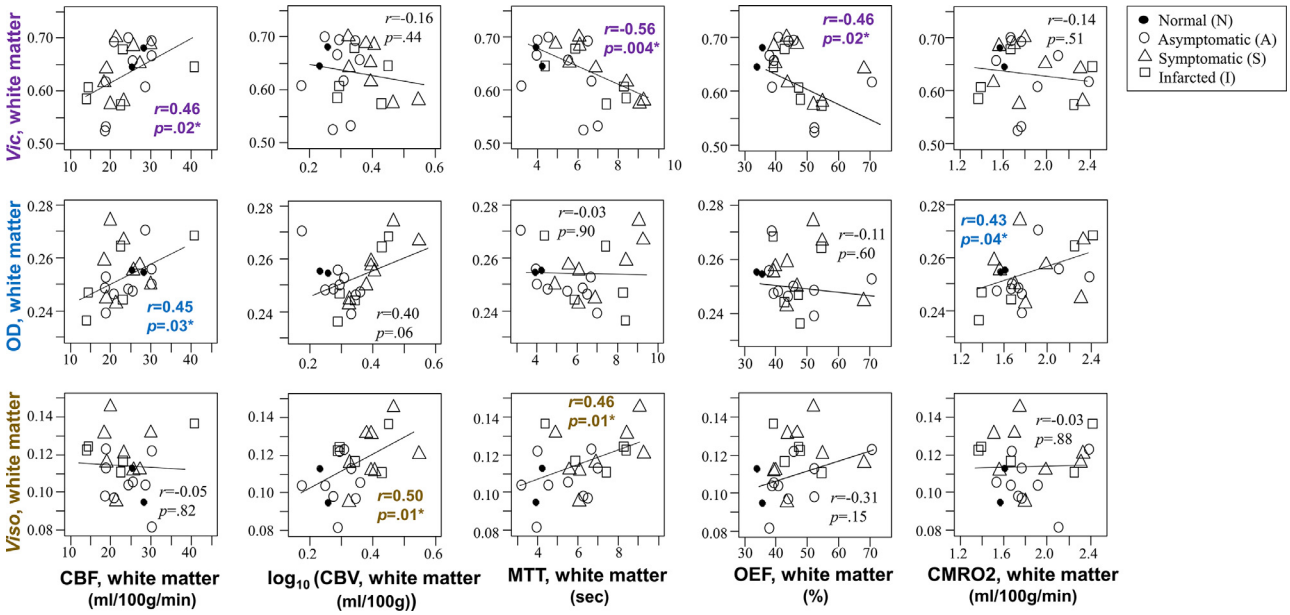

Figure 3. *The correlations among the parametric values of neurite orientation dispersion and density imaging (NODDI) and positron emission tomography (PET) in the white matter.*

*Intracellular volume fraction (V_{ic}) appeared to correlate better with the cerebral blood flow (CBF) and mean transit time (MTT) than with the orientation dispersion index (OD). The isotropic volume fraction (V_{iso}) was significantly correlated with the MTT and cerebral blood volume (CBV), which is similar to the correlation in the cortical areas. *P < .05 and †P < .05 after Bonferroni correction. CMRO2, cerebral metabolic rate of oxygen; OEF, oxygen extraction fraction; V_{ic}, intracellular volume fraction; cerebral blood volume.*

NODDI and Clinical Severity in Moyamoya Patients and Controls

As shown in Figure 4, the V_{ic}, OD and V_{iso} values in the cortical areas were significantly different among the 4 groups, and the OD values exhibited the most significant differences. In the white matter areas, the other 3 groups (eg, groups A, S, and I) showed significantly lower V_{ic} values than group N. The V_{iso} values in the more affected groups (eg, groups S, and I) were significantly higher than those in group N. The OD values in group I were significantly lower than those in the other groups, but no differences were observed among groups N, A, and S. The trend test confirmed that the V_{ic} and OD values were decreased, and the V_{iso} values were increased in both the cortical areas and white matter, as the clinical severity increased ($P < .001$ for all, remained significant after the Bonferroni correction). The presence of white matter hyperintensities and lesions was significantly lower in group N compared to other groups (Table 1, $P < .004$); however, there was no significant difference between groups A and S ($P = .94$).

There were no significant differences between the parametric values of the right and left hemispheres in either Moyamoya patients or normal volunteers ($P = .07$-$.90$, Supplementary Table 3). The age-NODDI analysis revealed a significant negative correlation between age and the cortical OD values ($r = -0.49$; $P = .001$), which was less apparent in the Moyamoya patients ($r = -0.18$; $P = .17$: Supplementary Figure 2 for details). A positive correlation was observed between age and white matter OD ($r = 0.65$; $P < .001$ vs. $r = 0.38$; $P = .002$) and cortical V_{iso} ($r = 0.64$: $P < .001$ vs. $r = 0.59$; $P < .001$) in both healthy volunteers and Moyamoya patients, but the correlation coefficient was relatively smaller in the Moyamoya patients. The adult-onset patients were older than childhood-onset patients and showed higher V_{iso} in the cortex and lower OD in the white matter (Supplementary Table 4).

NODDI and Neurocognitive Function in Moyamoya Patients

There was no significant difference between the PIQ and VIQ scores ($P = .13$, unpaired t test). Of the 4 index scores, the WM scores were significantly lower than the VC scores ($P = .01$, unpaired t test); however, no significant difference was observed when the 4 index scores were compared ($P = .06$-$.99$, T-K HSD test).

There was a significant correlation between the cortical V_{ic} and OD values and the FIQ, PIQ, PO, and PS scores (Table 2). In addition to these parameters, the white matter V_{ic} values correlated with the WM scores. However, the V_{iso} values did not correlate with any of the neurocognitive scores. Overall, the strongest correlation was observed between V_{ic} and PS, which remained significant after Bonferroni correction (Fig 5). The values obtained for the right and left hemispheres yielded similar results (Supplementary Table 7).

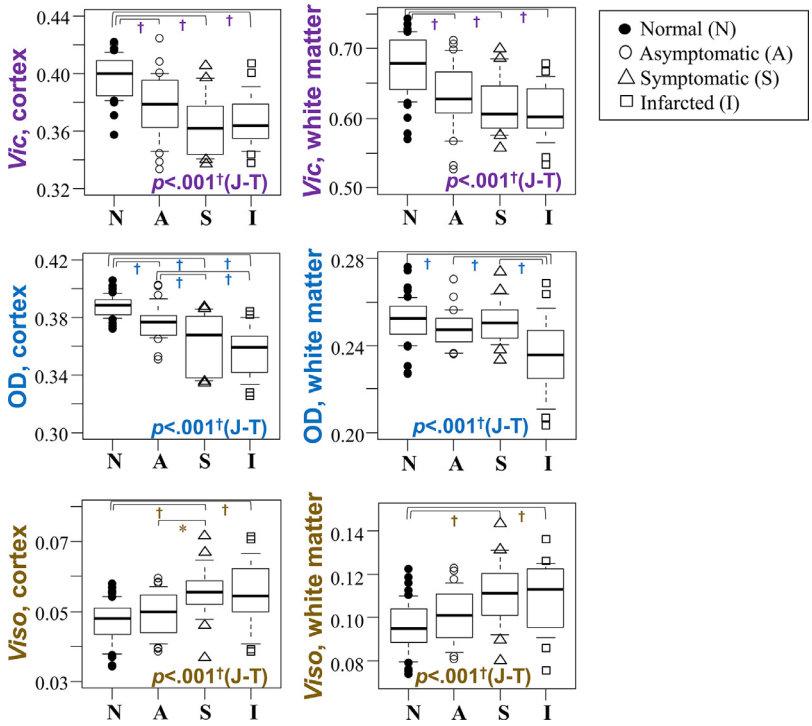

Figure 4. *The difference in neurite orientation dispersion and density imaging (NODDI) parameters among the four groups (ie, Groups N, A, S, and I) in the cortical area and in the white matter area.*

In the group assumed to be more affected and injured due to greater ischemia, the intracellular volume fraction (V_{ic}) and orientation dispersion index (OD) values were lower, and the isotropic volume fraction (V_{iso}) values were higher (P < .001 by Jonckheere-Terpstra trend test in all assessments). *P < .05 *and* †P < .05 *after Bonferroni correction.*

Table 2. *Correlation between the whole-brain NODDI values and WAIS-III scores. Of the 4 index scores, the WM scores were significantly lower than the VC scores. There was a significant correlation between the cortical intracellular volume fraction (V_{ic}) and orientation dispersion index (OD) values and the full-scale intelligence quotient (FIQ), performance IQ (PIQ), perceptual organization index (PO) and processing speed index (PS). In addition to these parameters, the white matter V_{ic} values correlated with the working memory index (WM). However, the isotropic volume fraction (V_{iso}) values did not correlate with any of the neurocognitive scores. Overall, the strongest correlation was observed between V_{ic} and PS, which remained significant after Bonferroni correction*

		FIQ	VIQ	PIQ	VC	PO	WM	PS
	Average (SD)	93 (19)	97 (18)	90 (17)	99 (15)	92 (18)	**88*** (15)**	91 (19)
	No. of patients <1 SD (%)	9 (29%)	8 (26%)	12 (39%)	6 (19%)	10 (32%)	12 (39%)	11 (35%)
	No. of patients <2 SD (%)	3 (10%)	2 (6%)	4 (13%)	0 (0%)	4 (13%)	4 (13%)	6 (19%)
Cortex	V_{ic}	0.33 (.07)	0.26 (.15)	**0.38 (.04*)**	0.16 (.41)	**0.40 (.02*)**	0.31 (.09)	**0.57 (<.001†)**
r (*p*)	OD	0.27 (.14)	0.16 (.40)	**0.37 (.04*)**	0.09 (.64)	**0.36 (.047*)**	0.36 (.17)	**0.51 (.003*)**
	V_{iso}	0.21 (.25)	0.30 (.10)	0.09 (.63)	0.32 (.70)	0.07 (.70)	0.07 (.30)	0.02 (.93)
White matter	V_{ic}	**0.45 (.01*)**	**0.39 (.03*)**	**0.48 (.006*)**	0.29 (.11)	**0.49 (.005*)**	**0.37 (.04*)**	**0.64 (<.001†)**
r (*p*)	OD	**0.40 (.03*)**	**0.42 (.02*)**	0.33 (.07)	0.32 (.08)	0.27 (.14)	0.27 (.14)	**0.37 (.04*)**
	V_{iso}	−0.05 (.77)	−0.02 (.93)	−0.10 (.59)	−0.14 (.45)	−0.14 (.65)	−0.08 (.96)	−0.09 (.64)

Abbreviations: SD, standard deviation; VC, verbal comprehension index; VIQ, verbal intelligence quotient.
*$P < .05$, and
†$P < .05$ after Bonferroni correction.

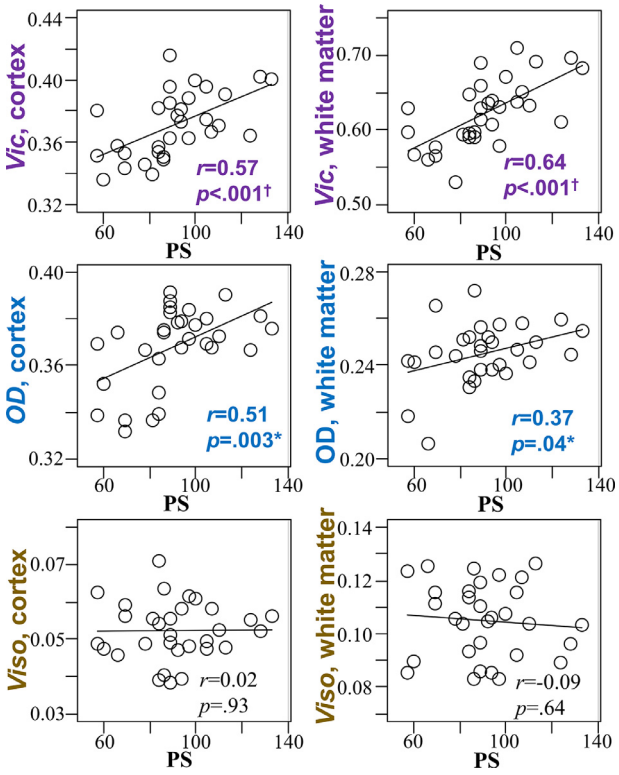

Figure 5. *Correlations between processing speed index (PS) and neurite orientation dispersion and density imaging (NODDI) parametric values for the whole cortex and white matter.*

*The intracellular volume fraction (V_{ic}) and orientation dispersion index (OD) values, but not the isotropic volume fraction (V_{iso}) values, were correlated with neurocognitive performance. The strongest correlation was observed between the white matter V_{ic} and PS. *P < .05 and †P < .05 after Bonferroni correction.*

Discussion

In summary, by comparing NODDI and PET parameters, we found that OD and V_{ic} values decreased and V_{iso} values increased as hemodynamic and metabolic parameters worsened. Subgroup analysis based on the symptomatically estimated severity of disease burden showed that as the clinical condition became more severe, the OD and V_{ic} values decreased more, and the V_{iso} values increased more in both the cortical and white matter regions. The OD and V_{ic} values positively correlated with the neurocognitive scores, and the strongest correlation was observed between the neurocognitive scores and the V_{ic} values of the white matter. The decrease in the V_{ic} values and the increase in the V_{iso} values were consistent with our prehypothesis and the reported decrease in the fractional anisotropy (FA) in patients with Moyamoya disease.[4]

Theoretically, OD should negatively correlate with FA,[5] and the decrease in OD was contradictory to our prehypothesis. This result may be explained by histological findings in animal studies suggesting that chronic ischemia induces bending and a reduced number of axons in the white matter and a reduced number of dendrites, dendritic spines, and branches in the cortex.[21] The additional analysis between PET and DTI parameters (Supplementary Table 4) also suggested that OD is superior to DTI parameters such as FA in terms of the correlation with CBF and MTT in the cortical areas. OD may not be a mere inverse parameter of FA and may instead reveal novel characteristics of brain microstructures that conventional diffusion MRI has failed to recognize, such as the shrinkage in dendritic processes.[22] The positive correlation between the V_{ic}, OD, and hemodynamic parameters of PET, the group difference among the clinical entities, and the correlation with the neuropsychological scores were all consistent with the sequelae of ischemic brain damage observed in Moyamoya disease—that is, a decrease of axons in white matter and the dendrites and dendritic processes in the cortex.

NODDI and PET

DTI and ^{18}F-2-fluoro-2-deoxy-D-glucose (FDG)-PET, which indicates the degree of neurosynaptic activity, are frequently used to investigate the relationship between cortical metabolism and the white matter microstructure. A direct correlation between FDG uptake and FA values has been observed in the posterior cingulate in patients with mild cognitive impairment.[23] Additionally, FDG uptake in the cortex is correlated with the FA values of the associated or adjacent white matter in healthy elderly subjects.[24] In these studies, the authors analyzed the relative uptake of FDG and did not quantify brain glucose metabolism; on the other hand, we used ^{15}O-gas PET in the present study, which is the gold standard for evaluating cerebral hemodynamics and metabolism, to provide quantitative values for oxygen metabolism (CMRO2), which is directly related to neuronal firing and correlate with neurocognitive dysfunction in Moyamoya disease.[25] Such a direct comparison between quantified biological PET parameters and the newly proposed NODDI parameters has not been performed previously. By quantitatively analyzing brain metabolism, we expected to identify a microstructural and metabolic correlation in our analysis, but unexpectedly, the correlation between V_{ic}/OD and CMRO2 was not as robust as the correlation between the hemodynamic parameters CBF and MTT. The superior correlation with hemodynamics compared with that of metabolism might suggest that ischemia induces microstructural changes from a very early stage, while metabolism remains preserved.[12] This theory is consistent with the differences of V_{ic}/OD observed between the normal-appearing brain (ie, group N) and the asymptomatic but affected hemispheres (ie, group A). Another possibility is that regional metabolism did not directly reflect regional microstructure because the regional microstructure could be affected by adjacent subcortical white matter lesions,[26] remote focal brain damage or the metabolic condition of the opposite hemisphere, such as in diaschisis.[27] The CBF values themselves may have affected the diffusion parametric values.[28]

In our study, V_{ic}/OD appeared to correlate better with the MTT than with CBF (Figs 2, 3). The MTT, which is inversely correlated with cerebral perfusion pressure,[12] is significantly elongated in the symptomatic and infarcted Moyamoya patients,[29,30] and also predicts the presence of misery perfusion[31] and the benefit and the risk of bypass surgery in Moyamoya patients.[32,33] An elongated MTT (ie, low CBF and a high CBV) may be the most sensitive indicator of impaired hemodynamics and microstructure in Moyamoya disease. These specific features of Moyamoya disease may underlie the robust correlation with MTT. However, notably, increased CBV and MTT are rarely observed in patients with atherosclerotic cerebrovascular disease[34]; therefore, the correlation between the PET and NODDI parameters demonstrated in Moyamoya disease may not be generalizable to all types of patients with chronic cerebral ischemia, such as patients with atherosclerotic occlusive cerebrovascular diseases.

NODDI and Clinical Severity

The cortical OD values exhibited the most significant difference among the groups, suggesting that this parameter is the most sensitive indicator of hemodynamic compromise. This finding is consistent with the robust correlation among CBF, MTT, and OD observed in the PET-NODDI analysis. In both the cortex and white matter, the V_{ic} and OD decreased as the clinical status became more severe, which again suggested a reduced number of neurons and axons and the complexity of the networks, as observed in the correlation with PET. The lack of a correlation between the cortical OD values and age in the Moyamoya patients (Supplementary Figure 2), which was observed in the healthy volunteers,[6] also suggested that the ischemic burden in Moyamoya disease has a stronger effect than aging on cortical microstructure.

In contrast to the cortical OD, the white matter OD did not stratify the disease burden in Moyamoya disease. The white matter OD values in Moyamoya patients showed only a moderate correlation with the white matter CBF (Fig 1), which was strongly correlated in the cortical areas (Fig 3) and did not correlate with the hemodynamic parameters of the adjacent cortex (Supplementary Table 2). Additionally, there was no difference between patients and healthy volunteers without infarctions (ie, groups N, A, and S), and the decrease in the OD was only significant in normal-appearing white matter in hemispheres harboring the infarction (Fig 4). The changes in the OD in the white matter may not be straightforward, ie, the tortuous axons and disrupted networks may cause a high dispersion, while the reduced number of axons caused by neuronal death and loss of fibers could simultaneously decrease the number of axonal networks and thus lead to a low dispersion. The white matter OD appeared to decrease only when the ischemic damage became excessive and the axonal loss became severe, as in the normally appearing part of the infarcted brain (ie, group I).

We believe that both the duration and severity of the hemodynamic compromise are important determinants of the brain microstructure because Moyamoya disease is not congenital and develops at some time during a patient's lifetime[1,35]; however, no difference in the NODDI parameters between childhood- and adulthood-onset groups was evident in our dataset (Supplementary Table 4). Some of the differences between the 2 groups appeared to be explained by the difference in the age distribution. Several studies have reported that adult-onset disease is less severe than pediatric-onset disease in the context of neurocognitive dysfunction and social outcome,[1] suggesting that ischemia during childhood has a negative impact on brain development and/or that a longer duration of ischemia results in increased brain microstructural damage. Additional cases must be assessed to clarify the effect of the disease duration.

NODDI and Neurocognitive Function

According to the analysis of the NODDI parameters and neurocognitive scores, the V_{ic} correlated better with WAIS-III scores than the OD, and the strongest correlation that remained significant after Bonferroni correction was observed between the white matter V_{ic} values and the PS scores. Several studies have suggested that PS decreases in neurological diseases that primarily affect the white matter diseases.[36,37] Additionally, the white matter FA values were correlated with the PS in normal elderly people.[38] Considering those studies suggesting that white matter damage is more prominent than cortical injury in animals with chronic ischemia, the longstanding ischemia in Moyamoya disease may primarily affect the white matter integrity, decrease axonal density, and thus lead to inefficient communication inside the brain, ie, decreased PS. The decreased V_{ic} and PS scores may represent sensitive biomarkers for evaluating the severity of chronic ischemia. Moreover, considering that even asymptomatic hemispheres exhibited significant differences in V_{ic} and OD values compared with those of normal hemispheres and that V_{ic} and OD correlated with neurocognitive performance, surgical intervention may be warranted, even in the asymptomatic hemisphere, to prevent neurocognitive dysfunction due to chronic ischemia in patients with Moyamoya disease.

Interestingly, the V_{iso} correlated well with the hemodynamic parameters (eg, CBF, MTT, and CBV) of PET and the V_{ic} and OD but not with neurocognitive function. These differences suggest that the increase in V_{iso} is not identical to the decrease in V_{ic} as theoretically indicated. The increased parenchymal water is likely directly unrelated to the decrease in the neurite fraction, and a possible and attractive explanation is that the increased parenchymal water is due to a dysfunction in the glymphatic system,[39] which is driven by

arterial pulsatility[40] and is speculated to be impaired in patients with Moyamoya disease.[41] The increase in the apparent diffusion coefficient in the hemodynamically impaired white matter of Moyamoya disease,[42] the reversibility of some white matter lesions after the restoration of the hemodynamic compromise by bypass surgery in Moyamoya disease[43] and extracranial carotid artery stenosis,[44] the regression of the white matter lesions after acute ischemic stroke,[45] and the improvement in diabetic status[46] might all be related to this mechanism, ie, impaired CSF circulation. Another possibility is that the slow movement of water molecules in the dilated capillaries and small vessels is mistakenly calculated as interstitial fluid and leads to an overestimation of the V_{iso}, considering the correlation observed between the V_{iso} and CBV (Figs 1, 2). Using another method to calculate the interstitial water component (eg, T1 map), assessing the effect of the perfusion fraction,[28] and evaluating atherosclerotic cerebrovascular diseases in which the CBV usually does not increase as much as that in Moyamoya disease could further clarify the significance of the V_{iso}.

Although Moyamoya disease commonly affects the anterior circulation of the brain from the early stage and although patients are generally assumed to have frontal lobe dysfunction,[1,4] the correlation between the NODDI parameters and the WM was poor. The uniform relative decline in frontal lobe function likely led to the poor microstructural-functional correlations in the patients. Further analysis of the relationship between neurocognition and regional differences in NODDI parameters is needed since the FA values of the specific fiber originating from the frontal lobe correlate with frontal lobe dysfunction in Moyamoya disease.[4]

The lateralization effect of the hemispheres was not apparent in our analysis between NODDI and neurocognitive function, although the left side was presumed to be the dominant hemisphere for most participants. Some patients may have experienced a functional shift in neurocognition to the healthy side[47] because of local brain damage caused by infarction and hemorrhage. Considering the complexity and heterogeneity of the hemodynamic impairment that accompanies Moyamoya disease, we believe it would be better to evaluate the whole-brain average value instead of the unilateral hemispheric values to assess the degree of brain ischemic damage and its impact on cognitive function in patients with this disease.

Limitations and Perspectives

Our study is limited by relatively small number of patients, considering the heterogeneity of the clinical presentation, the selection method of PET candidates and the lack of PET data on normal controls. We used hemispheric and whole-brain values to determine the broad structure of the ischemic-microstructural relationship; therefore, intraregional differences in the PET[20] and NODDI parameters[6] were not considered. We believe that interpreting regional differences using this small sample size will still be difficult. We created cortical and white matter region of interests to minimize the partial volume effect and mixed effects, which resulted in missed information regarding the subcortical white matter adjacent to the cortex. We included 2 hemispheres of each patient in our analysis with PET and clinical severity, considering that the hemodynamic and metabolic statuses of the 2 hemispheres are highly variable in patients with Moyamoya disease; however, there may be some remote effect from contralateral hemisphere to the hemodynamic and metabolic status from contralateral hemisphere, beyond local microstructures. It is unclear whether the specific microstructural ischemic damage suggested in this study is generally applicable to the patients with other diseases causing chronic ischemia, such as atherosclerotic occlusive cerebrovascular diseases, which, to the best our knowledge, has not been reported so far. Conventional diffusion parameters calculated via simple mathematical models may be more robust and sensitive than NODDI, at least in white matter areas (Supplementary Table 4); however, NODDI is superior to conventional diffusion metrics in the sense that the parameters reveal specific histological findings, whereas conventional diffusion parameters such as FA do not.

Further evaluations involving large patient cohorts, eg, elucidation of regional parametric differences associated with hemodynamics and neurocognitive function, determination of whether the reversal of microstructural damage can be observed after the restoration of ischemia by bypass surgery, and assessment of the differences with atherosclerotic cerebrovascular diseases, are expected to establish the clinical feasibility of NODDI in patients with Moyamoya disease.

Conclusions

NODDI was able to illustrate the specific microstructural damage induced by chronic ischemia in patients with Moyamoya disease; this damage was correlated with the quantitative parameters of cerebral perfusion and metabolism obtained using ^{15}O-gas PET, the clinical profile of the patients, and neurocognitive dysfunction. Noninvasive NODDI might be used to predict the degree of ischemic burden before applying invasive PET studies to patients with Moyamoya disease.

Competing Interests

The authors declared no potential conflicts of interest with respect to the research, authorship, and/or publication of this article.

Acknowledgments: The authors would like to thank Tokyo Medical Clinic for the MRI acquisition, Team for Neuroimaging Research in Tokyo Metropolitan Institute of Gerontology for the PET measurements and analyses, Ai Hirabayashi for suggestions concerning the neurophysiological evaluation,

Masako Akiyama for statistical guidance, and Maki Mukawa for gene analysis.

Supplementary Material

Supplementary data to this article can be found online at doi:10.1016/j.jstrokecerebrovasdis.2018.12.038.

References

1. Guidelines for diagnosis and treatment of Moyamoya disease (spontaneous occlusion of the circle of Willis). Neurol Med Chir (Tokyo) 2012;52:245-266.
2. Karzmark P, Zeifert PD, Bell-Stephens TE, et al. Neurocognitive impairment in adults with Moyamoya disease without stroke. Neurosurgery 2012;70:634-638.
3. Hara S, Hori M, Murata S, et al. Microstructural Damage in normal-appearing brain parenchyma and neurocognitive dysfunction in adult Moyamoya disease. Stroke 2018;49:2504-2507.
4. Kazumata K, Tha KK, Narita H, et al. Chronic ischemia alters brain microstructural integrity and cognitive performance in adult Moyamoya disease. Stroke 2015;46:354-360.
5. Zhang H, Schneider T, Wheeler-Kingshott CA, et al. NODDI: practical in vivo neurite orientation dispersion and density imaging of the human brain. Neuroimage 2012;61:1000-1016.
6. Kodiweera C, Alexander AL, Harezlak J, et al. Age effects and sex differences in human brain white matter of young to middle-aged adults: a DTI, NODDI, and q-space study. Neuroimage 2016;128:180-192.
7. Sato K, Kerever A, Kamagata K, et al. Understanding microstructure of the brain by comparison of neurite orientation dispersion and density imaging (NODDI) with transparent mouse brain. Acta Radiologica Open 2017;6:2058460117703816.
8. Adluru G, Gur Y, Anderson JS, et al. Assessment of white matter microstructure in stroke patients using NODDI. Conf Proc IEEE Eng Med Biol Soc 2014;2014:742-745.
9. Kamagata K, Zalesky A, Hatano T, et al. Gray matter abnormalities in idiopathic parkinson's disease: evaluation by diffusional kurtosis imaging and neurite orientation dispersion and density imaging. Hum Brain Mapp 2017;38:3704-3722.
10. Irie R, Tsuruta K, Hori M, et al. Neurite orientation dispersion and density imaging for evaluation of corticospinal tract in idiopathic normal pressure hydrocephalus. Jpn J Radiol 2016;35:25-30.
11. Nazeri A, Mulsant BH, Rajji TK, et al. Gray matter neuritic microstructure deficits in schizophrenia and bipolar disorder. Biol Psychiatry 2016;82:726-736.
12. Powers WJ, Grubb Jr. RL, Raichle ME. Physiological responses to focal cerebral ischemia in humans. Ann Neurol 1984;16:546-552.
13. Andersson JL, Skare S, Ashburner J. How to correct susceptibility distortions in spin-echo echo-planar images: application to diffusion tensor imaging. Neuroimage 2003;20:870-888.
14. Smith SM, Jenkinson M, Woolrich MW, et al. Advances in functional and structural MR image analysis and implementation as FSL. Neuroimage 2004;23(Suppl 1):S208-S219.
15. Shidahara M, Watabe H, Kim KM, et al. Optimal scan time of oxygen-15-labeled gas inhalation autoradiographic method for measurement of cerebral oxygen extraction fraction and cerebral oxygen metabolic rate. Ann Nucl Med 2008;22:667-675.
16. Kudomi N, Choi E, Yamamoto S, et al. Development of a GSO detector assembly for a continuous blood sampling system. IEEE T Nucl Sci 2003;50:70-73.
17. Miwa K, Umeda T, Murata T, et al. Evaluation of scatter limitation correction: a new method of correcting photopenic artifacts caused by patient motion during whole-body PET/CT imaging. Nucl Med Commun 2016;37:147-154.
18. Shidahara M, Watabe H, Kim KM, et al. Evaluation of a commercial PET tomograph-based system for the quantitative assessment of rCBF, rOEF and rCMRO2 by using sequential administration of 15O-labeled compounds. Ann Nucl Med 2002;16:317-327.
19. Saha GB. Performance Characteristics of PET Scanners. Basics of PET Imaging: Physics, Chemistry, and Regulations. Cham: Springer International Publishing; 2016. 121-142.
20. Nariai T, Matsushima Y, Imae S, et al. Severe haemodynamic stress in selected subtypes of patients with moyamoya disease: a positron emission tomography study. J Neurol Neurosurg Psychiatry 2005;76:663-669.
21. Farkas E, Luiten PG, Bari F. Permanent, bilateral common carotid artery occlusion in the rat: a model for chronic cerebral hypoperfusion-related neurodegenerative diseases. Brain Res Rev 2007;54:162-180.
22. Parker TD, Slattery CF, Zhang J, et al. Cortical microstructure in young onset Alzheimer's disease using neurite orientation dispersion and density imaging. Hum Brain Mapp 2018;39:3005-3017.
23. Walhovd KB, Fjell AM, Amlien I, et al. Multimodal imaging in mild cognitive impairment: metabolism, morphometry and diffusion of the temporal-parietal memory network. Neuroimage 2009;45:215-223.
24. Inoue K, Ito H, Uchida S, Taki Y, et al. Decrease in glucose metabolism in frontal cortex associated with deterioration of microstructure of corpus callosum measured by diffusion tensor imaging in healthy elderly. Hum Brain Mapp 2008;29:375-384.
25. Hosoda C, Nariai T, Ishiwata K, et al. Correlation between focal brain metabolism and higher brain function in patients with Moyamoya disease. Int J Stroke 2010;5:367-373.
26. DeCarli C, Murphy DG, Tranh M, et al. The effect of white matter hyperintensity volume on brain structure, cognitive performance, and cerebral metabolism of glucose in 51 healthy adults. Neurology 1995;45:2077-2084.
27. Iglesias S, Marchal G, Rioux P, et al. Do changes in oxygen metabolism in the unaffected cerebral hemisphere underlie early neurological recovery after stroke? A positron emission tomography study. Stroke 1996;27:1192-1199.
28. Urushihata T, Takuwa H, Seki C, et al. Water diffusion in the brain of chronic hypoperfusion model mice: a study considering the effect of blood flow. Magn Reson Med Sci 2018;17:318-324.
29. Hirai S, Inaji M, Tanaka Y, et al. Correlation between clinical presentations and hemodynamic parameters measured by dynamic susceptibility contrast magnetic resonance imaging in adult patients with Moyamoya disease. J Stroke Cerebrovasc Dis 2017;26:2814-2820.
30. Hara S, Tanaka Y, Ueda Y, et al. Noninvasive evaluation of CBF and perfusion delay of Moyamoya disease using arterial spin-labeling MRI with multiple postlabeling delays: comparison with 15O-Gas PET and DSC-MRI. AJNR Am J Neuroradiol 2017;38:696-702.

31. Tanaka Y, Nariai T, Nagaoka T, et al. Quantitative evaluation of cerebral hemodynamics in patients with Moyamoya disease by dynamic susceptibility contrast magnetic resonance imaging—comparison with positron emission tomography. J Cereb Blood Flow Metab 2006;26:291-300.
32. Ishii Y, Nariai T, Tanaka Y, et al. Practical clinical use of dynamic susceptibility contrast magnetic resonance imaging for the surgical treatment of Moyamoya disease. Neurosurgery 2014;74:302-309.
33. Karakama J, Nariai T, Hara S, et al. Unique angiographic appearances of Moyamoya disease detected with 3-dimensional rotational digital subtraction angiography imaging showing the hemodynamic status. J Stroke Cerebrovasc Dis 2018;27:2147-2157.
34. Derdeyn CP, Videen TO, Yundt KD, et al. Variability of cerebral blood volume and oxygen extraction: stages of cerebral haemodynamic impairment revisited. Brain 2002;125:595-607.
35. Aoyama J, Nariai T, Mukawa M, et al. A case of familial Moyamoya disease presenting 10 years after the initial negative MR screening in childhood. World Neurosurg 2017;105:1035.e1-1035.e4. (https://www.ncbi.nlm.nih.gov/pubmed/28619492).
36. Duering M, Gesierich B, Seiler S, et al. Strategic white matter tracts for processing speed deficits in age-related small vessel disease. Neurology 2014;82:1946-1950.
37. Kennedy JE, Clement PF, Curtiss G. WAIS-III processing speed index scores after TBI: the influence of working memory, psychomotor speed and perceptual processing. Clin Neuropsychol 2003;17:303-307.
38. Turken A, Whitfield-Gabrieli S, Bammer R, et al. Cognitive processing speed and the structure of white matter pathways: convergent evidence from normal variation and lesion studies. Neuroimage 2008;42:1032-1044.
39. Taoka T, Masutani Y, Kawai H, et al. Evaluation of glymphatic system activity with the diffusion MR technique: diffusion tensor image analysis along the perivascular space (DTI-ALPS) in Alzheimer's disease cases. Jpn J Radiol 2017;35:172-178.
40. Iliff JJ, Wang M, Zeppenfeld DM, et al. Cerebral arterial pulsation drives paravascular CSF-interstitial fluid exchange in the murine brain. J Neurosci 2013;33:18190-18199.
41. Hara S, Hori M, Inaji M, et al. Regression of white matter hyperintensity after restoration of severe hemodynamic impairment in a patient with Moyamoya disease. Magn Reson Med Sci 2018. https://doi.org/10.2463/mrms.ci.2018-0088. [Epub ahead of print].
42. Conklin J, Fierstra J, Crawley AP, et al. Impaired cerebrovascular reactivity with steal phenomenon is associated with increased diffusion in white matter of patients with Moyamoya disease. Stroke 2010;41:1610-1616.
43. Komatsu K, Mikami T, Noshiro S, et al. Reversibility of white matter hyperintensity by revascularization surgery in Moyamoya disease. J Stroke Cerebrovasc Dis 2016;25:1495-1502.
44. Yamada K, Sakai K, Owada K, et al. Cerebral white matter lesions may be partially reversible in patients with carotid artery stenosis. Am J Neuroradiol 2010;31:1350-1352.
45. Cho AH, Kim H-R, Kim W, Yang DW. White matter hyperintensity in ischemic stroke patients: it may regress over time. J Stroke 2015;17:60-66.
46. Adachi M, Sato T. Characterization of the growth of deep and subcortical white matter hyperintensity on MR imaging: a retrospective cohort study. Magn Reson Med Sci 2017;16:238-244.
47. Wang L, Yu C, Chen H, et al. Dynamic functional reorganization of the motor execution network after stroke. Brain 2010;133:1224-1238.